Acústica 2020
XI Congreso Ibérico de Acústica
51º Congreso Español de Acústica
TECNIACÚSTICA 2020

VORTICES FOR BIOMEDICAL ULTRASOUND APPLICATIONS

Noé Jiménez [1,*], Sergio Jiménez-Gambín [1], Diana Andrés [1], Francisco Camarena[1]

[1] Instituto de Instrumentación para Imagen Molecular (I3M), Consejo Superior de Investigaciones Científicas - Universitat Politècnica de València, València, Spain
* e-mail: nojigon@upv.es

Resumen
Los vórtices acústicos contienen singularidades de fase y transportan, además de momento lineal, pseudomomento angular. El campo acústico de estos haces presenta una singular distribución espacial que los hace únicos para determinadas aplicaciones biomédicas, con particular interés para las basadas en fuerza de radiación acústica. En este trabajo presentamos el uso de hologramas acústicos y lentes de fase para generar múltiples haces focalizados de vórtice para su empleo en varias aplicaciones biomédicas. Primero, presentamos lo focalización transcraneal de haces de vórtice en el interior del cerebro, diseñados para atrapar y manipular pequeñas partículas como coágulos en el sistema nervioso central o el guiado y administración de fármacos. En segundo lugar, presentamos el empleo de haces de vórtice para de la transferir momento angular orbital al tejido blando. Ello produce un esfuerzo de torsión cuya dirección de rotación se puede controlar mediante el haz de vórtice modificando la carga topológica del mismo. Bajo una excitación transitoria los esfuerzos de torsión generan ondas transversales de polarización controlada. La detección de las ondas con un sistema de elastografía ultra rápido permite la obtención de las propiedades viscoelásticas del tejido de una manera robusta. Los vórtices acústicos ofrecen una manera única de interactuar con los tejidos biológicos, lo que permite el desarrollo de innovadoras aplicaciones biomédicas.

Palabras clave: Vórtices, Fuerza de Radiación, Levitación, Elastografía, Transcraneal.

Abstract
Acoustic vortices containing phase singularities carry, in addition to linear, angular pseudo-momentum. The singular spatial distribution of these beams makes them unique for selected biomedical applications including acoustic-radiation-force-based applications. We report the use of acoustic holograms and phase-plates to generate multiple focused vortex beams in several configurations. First, we present the transcranial focusing of vortex beams inside the brain to trap and manipulate of small particles and clots into the central-nervous system. Second, we report the transfer of orbital angular momentum to soft-tissue to produce transient torques of alternating direction of rotation, which leads to the generation of controlled-polarization of shear waves for elastographic imaging. The detection of shear waves with an ultra-fast elastography system allows to obtain the viscoelastic properties of the tissue in a robust way. Acoustic vortices offer a unique way to interact with biological tissues, allowing the development of groundbreaking biomedical applications.

Keywords: Vortex, Acoustic Radiation Force, Levitation, Elastography, Transcranial.

PACS nº. 43.80.Sh, 43.60.Sx

1 Introduction

Beyond the linear momentum carried by focused ultrasound beams, acoustic vortex beams carry angular orbital momentum [1]. Acoustic vortex beams are wavefronts containing phase dislocations as $\exp(il\phi)$, with ϕ the azimuthal angle and l the topological charge. The field presents a phase singularity at the axis of the beam, exhibiting at this point a null caused by destructive interferences. It has been demonstrated that the angular momentum carried by an acoustic vortex beam can be transferred to micro and macroscopic solid objects [2] or viscous fluids [3], exerting mechanical torques to these media. In addition, vortex beams induce trapping acoustic radiation forces on small particles, leading to particle tweezing and manipulation systems [4]–[6]. These acoustic vortices can exert mechanical forces several orders of magnitude higher than those of their optical counterparts, with lower induced thermal effects [7], and, furthermore, acoustic vortices can propagate deeply through opaque media such as biological tissues. Acoustic vortices have recently shown their potential for biomedical applications to manipulate individual cells without inducing photothermal and/or photochemical damages [8], to trap and guide kidney stones fragments in-vivo [9], or to selectively guide individual drug-delivery carriers based on microbubbles [10].

As phase dislocations are at the basis of these techniques, the wavefront must be controlled with accuracy. Several methods to synthesize vortex beams have been reported, including active sources or phased arrays systems and transducers with helical geometries [11], Archimedean [12] or Fresnel spiral diffraction gratings [13], systems exploiting the photoacoustic effect [14], active vibrating surfaces with spiral shape [15], or metamaterials exhibiting local resonances [16]. Of special interest for wavefront engineering are acoustic holograms [17]. By synthesizing complex wavefronts, acoustic holograms can efficiently compensate skull aberrations and, simultaneously, conform arbitrary acoustic images adapting to the desired therapeutic target [18], [19]. Acoustic holograms can be used to generate vortex beams with great accuracy by encoding the full-wavefront information into an array or a 3D printed lens [20].

In this work, we present the use of acoustic vortices for two applications. The first is to focus an ultrasonic vortex inside the human skull using hologram. Using personalized 3D printed holograms, the phase aberrations produced by the skull can be compensated and an acoustic beam containing phase dislocations can be focused into the cranial cavity. The second application is the use of the transfer of angular momentum of a vortex to twist and generate displacement in soft tissue. This allows to design elastographic techniques that outperform traditional approaches based in pushing acoustic radiation force.

2 Focusing ultrasonic vortices inside the human skull

The system is composed of a spherically focused piezoelectric transducer, custom made with a focal length of $F_0 = 140$ mm and an aperture of $2a_0 = 100$ mm, with a nominal frequency of $f_0 = 500$ kHz, as sketched in Fig. 1 (a).

To design the hologram including the aberrating layer of the skull we make use of a time-reversal method. The process essentially follows the procedure described in Ref. [18]. We start by scanning an ex-vivo human skull using x-ray CT with a resolution of $0.33 \times 0.33 \times 1.25$ mm^3, after the scalp was removed whole with a scalpel. Volumetric Hounsfield data was converted to bone density and sound speed values using empirical relations. Then, this tomographic information was used for a time-reversal simulation based on pseudo-spectral time-domain methods, including a *k*-space corrector and a spectral approximation of the fractional Laplacian to model the frequency power-law attenuation observed in biological tissues [21]. For the backward simulation step of the time-reversal approach, a set of 30 virtual sources were located along a ring of radius $r_s = 2.5$ mm at the plane $z_s = F = 97.4$ mm, as sketched in Fig. 1 (a). Each source was set to emit a sinusoidal signal with a complex

amplitude proportional to $\exp(il\theta)$. Then, the acoustic field $H_0(x, y)$ was recorded at the holographic plane located at the exit plane of the transducer, given by $z_0 = F_0 - (F_0^2 - a_0^2)^{1/2}$, resulting in the phase distribution shown in Fig. 1 (b). To compensate the geometrical focusing of the bowl source (note $F \neq F_0$), we set an additional simulation for the focused source in the absence of skull, and we measure the field $H_s(x, y)$ at the exit plane z_0. The retrieved phase distribution is shown in Fig. 1 (c), showing the characteristic Fresnel rings. Finally, the phase-conjugated hologram at the holographic plane is given by $H = H_0^* H_s^*$, where $(\cdot)^*$ denotes complex conjugation.

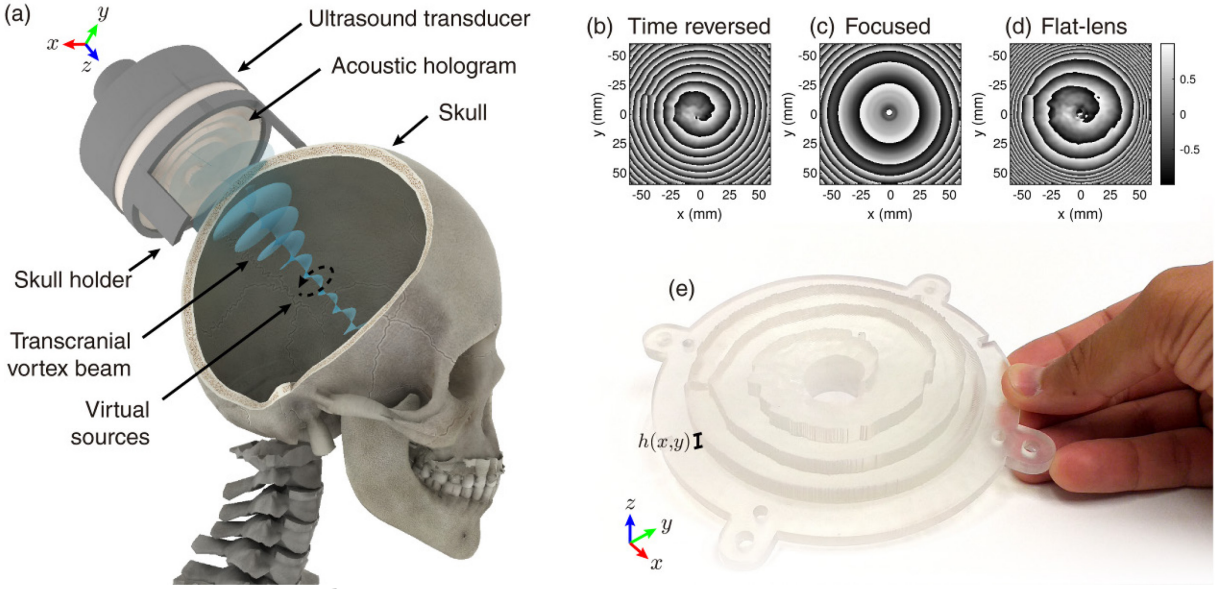


Figure 1. Vortex hologram ($l = 1$) designed for heterogeneous media. (a) Schematic of the approach. (b,c) Phase of the wavefront generated at the holographic surface by the virtual sources and by the focused transducer, respectively. (d) Phase-conjugated of the wavefront to design the lens obtained from the combination of (b) and (c). (e) 3D printed lens.

Figure 2 (a) shows the experimental setup, where the skull was immersed in a water tank and the acoustic field was scanned in several planes using a hydrophone. A skull holder was 3D printed to grant the correct positioning of the lens with respect to the surface of the skull. The irregular shape of the skull ensures that the holder can only be correctly located at the design position. The retrieved acoustic field is shown in Fig. 2 (b, c) for the simulation and experiment, respectively. The phase-only hologram can encode the time-reversed field with great accuracy. It compensates the aberrations of the skull while, simultaneously, modifying the wavefront to generate a focused vortex by introducing quasi-parabolic phase profile with rotational profile.

In addition, simulation and experimental results are in good agreement. The pressure peaks at $z = 96.9$ mm for the simulation and $z = 97.5$ mm for the experiment. The transversal field cross-sections at $z = F$ are shown in Figs. 2 (d-g). The transversal field magnitude [Figs. 2 (d,e)] shows a ring-shaped distribution like the one obtained for homogeneous media. The magnitude of the field vanishes at the center for both experimental and simulated results. The corresponding phase distribution is shown in Fig. 2 (f,g). The counterclockwise rotation is achieved at the focal plane, and a phase singularity is visible at the location of the null.

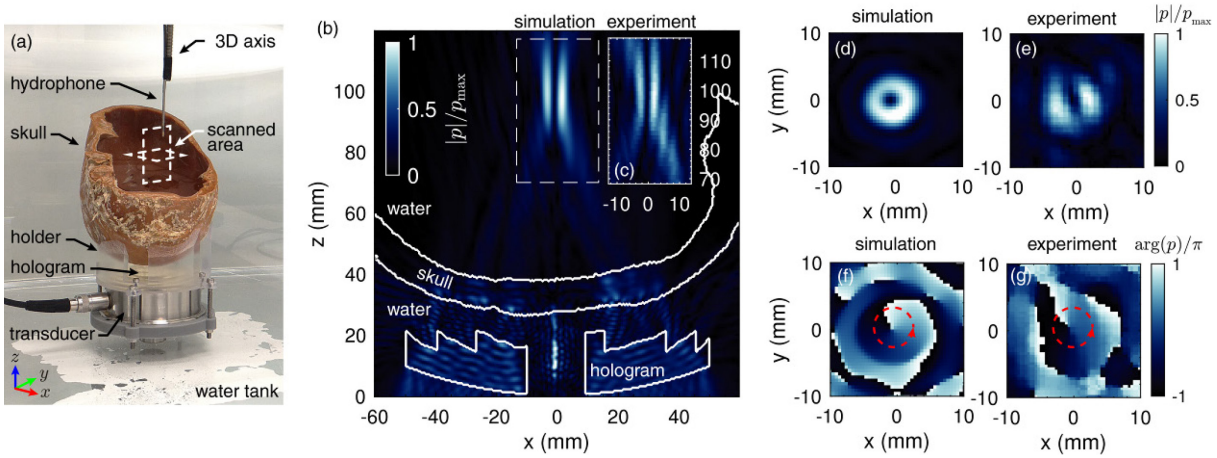


Figure 2. Field of the vortex hologram ($l = 1$) designed for transcranial propagation media. (a) Scheme of the experimental setup. (b) Simulated and (c) experimental normalized sagittal field cross-section at $y = 0$. (d,e) Magnitude and (f,g) phase of a transversal cross-section of the field obtained at $z = F$.

3 Vortex elastography

In this section, we present a novel method of elastography based on acoustic vortices to transfer angular momentum to tissue in addition to linear momentum. Focused vortex beams can push and twist tissue, and the rotation direction of the applied torque can be dynamically controlled by the modulation of the topological charge of the vortex. The technique results in a robust excitation of shear waves with quasi-omnidirectional radiation pattern and arbitrary waveform, which may have a great impact in imaging performance for elastography.

A focused vortex beam is generated by a ring-shaped piezoelectric focused source (H105, Sonic Concepts), with a focal of $F = 64$ mm, and outer and inner apertures of 64 mm and 37 mm, respectively, and a central frequency of $f = 1.1$ MHz. An helicoidal phase-plate lens that allows the selection of the topological charge of the vortex was 3D printed in photo-reactive polymer by stereolithography (Form2, Formlabs), and coupled with vacuum grease to the matching layer of the transducer. The lens was manufactured with a single topological charge, $l = 1$, as shown in Figs. 3 (a,b). A 64-elements phased-array piezoelectric probe (H105, Sonic Concepts) is mounted concentrically.

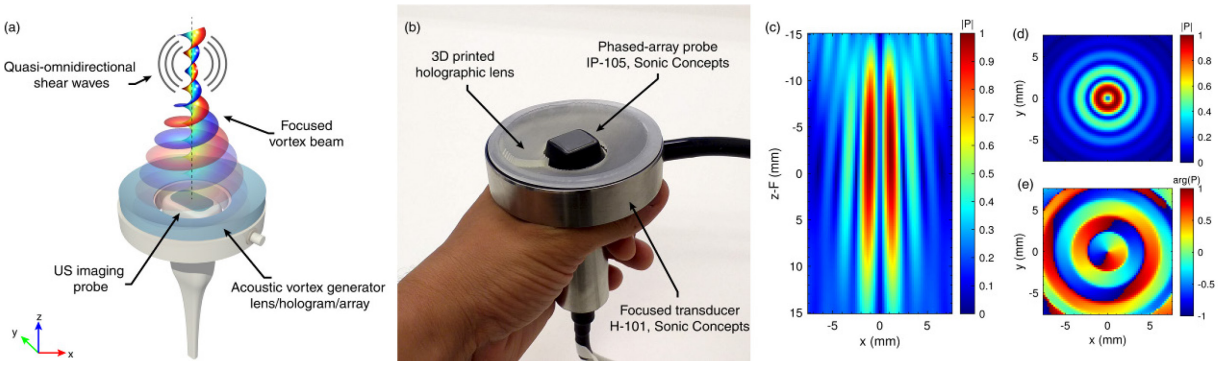


Figure 3. (a) Conceptual design of vortex-elastography systems, where the vortex generator can be implemented by a lens, a hologram, or a phased-array probe. (b) Implementation using a 3D printed lens for the vortex generator and a 64-elements phased array probe for the imaging system. (c) Magnitude of the calculated pressure field in the $p = p(x, 0, z)$ plane. (d) Magnitude and (e) phase of the calculated pressure field in the transverse $p = p(x, y, F)$ plane.

First, the theoretical field of the primary beam generated by the lens in water shows a phase dislocation on the axis and a topological charge $l = 1$, as shown in Figs. 3 (c-e). The system presents a linear gain of 16.0 and the distance between maxima, i.e., the width of the toroidal focus, is 1.7 mm.

Second, we theoretically calculate the acoustic radiation forces. When an absorbing tissue phantom of 0.5 dB/cm/MHz is introduced, a force appears because of an energy density gradient. The components of the force are shown in Fig. 4. In Fig. 4 (a) the axial component in the plane $(x, 0, z)$, is plotted normalized ($F_z/F_{\max}$), and the normalized lateral components of the force in the plane(x, y, F), $F_x/F_{\max}$ and $F_y/F_{\max}$, are shown in Figs. 4 (b, c), respectively. Finally, the acoustic radiation torque exerted in the tissue in the plane (x, y, F), $F_\theta/F_{\max}$ is shown in Fig. 4 (d) and Fig. 4 (e) shows the direction of the resulting force in the transverse plane (x, y, F). It is shown that for this focusing, the rotational component is about 3 times smaller than the axial component. Sharper focusing or higher topological charges can improve this ratio.

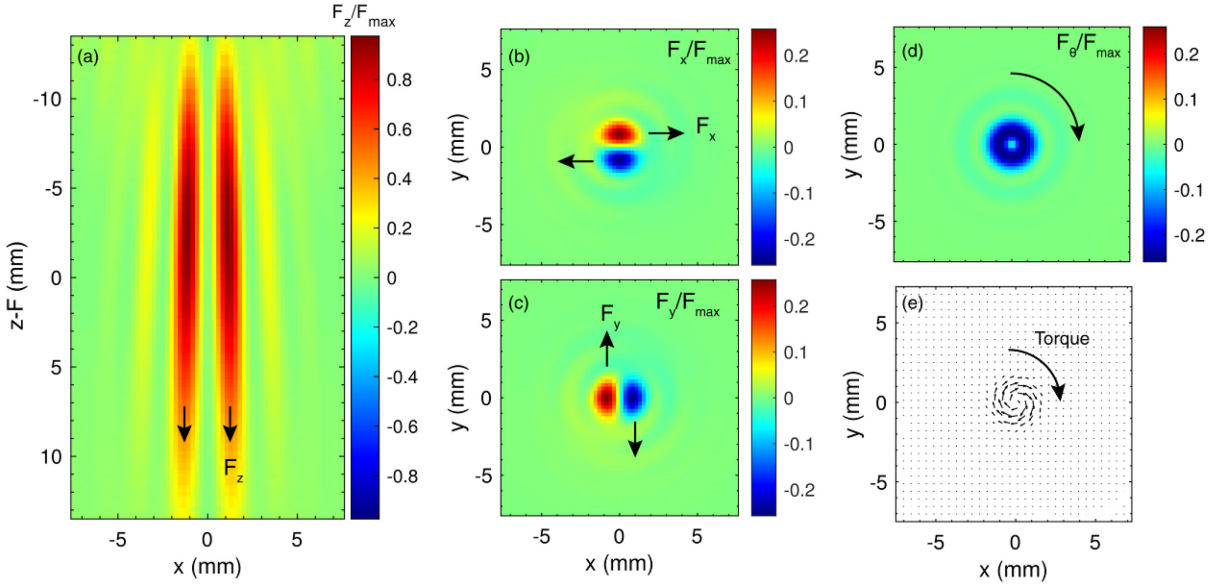


Figure 4. Acoustic radiation force calculated from the acoustic field in the soft tissue model. (a) Axial component in the plane $(x, 0, z)$, normalized ($F_z/F_{\max}$). (b,c) Normalized lateral components in the plane (x, y, F), $F_x/F_{\max}$ and $F_y/F_{\max}$, respectively. (d) Acoustic radiation torque exerted in the tissue in the plane (x, y, F), $F_\theta/F_{\max}$ and (e) vector field in the plane (x, y, F) showing the direction of the resulting force in the transverse plane.

Finally, vortex elastography is used for shear-wave dispersion ultrasound vibrometry. A sine-sweep modulated signal is applied to the primary ultrasound emitter for frequencies sweeping from $f_0 = 150$ Hz to $f_1 = 800$ Hz, and $T = 37$ ms is the duration of the sine-sweep pulse. In addition, the polarity of the topological charge is modulated using a phased-array vortex emitter in the simulation as

$$l(t) = l_0 \operatorname{sign}\left[\sin\left(2\pi\left[\frac{f_1 - f_0}{2T}t^2 + f_0 t\right]t\right)\right], \tag{1}$$

where $l_0 = 4$ is the magnitude of the topological charge, as shown in Figs 5 (a,b). The displacements are measured along the x direction, a sample is shown in Fig. 5 (c), where it can be observed the sine-sweep waveform retrieved in the simulations for the displacements in the y direction. Then, the spatiotemporal data is transformed to the $k - \omega$ frequency domain using a 2D Fast Fourier Transform. In this way, the dispersion relation of the phantom is obtained. The modes corresponding to the theoretical dispersion relation, given for this elastic phantom by the linear function $\omega(k) = c_0 k$, are shown by the colormap in Fig. 5 (d). It can be observed that the reconstructed modes belong to the theoretical dispersion relation, marked as a white dashed line.

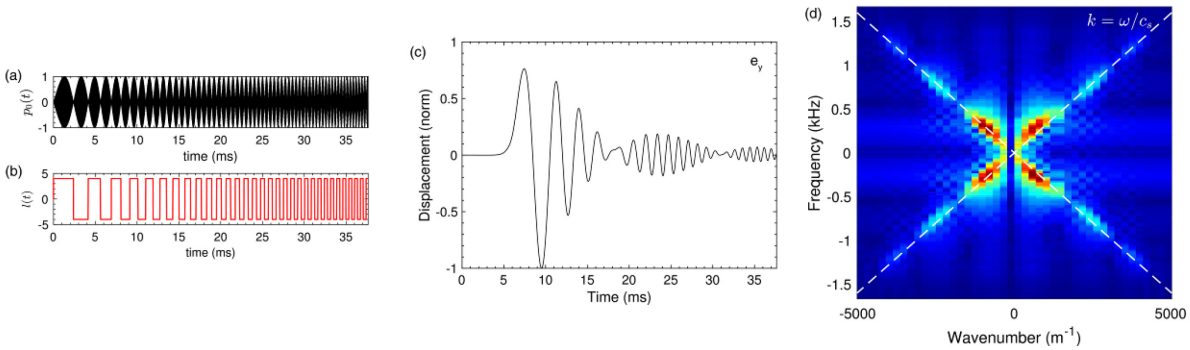


Figure 5. Example of application of the modulation of the topological charge to obtain the elastic properties of the medium as a function of the frequency. (a) Modulation signal for the primary field. (b) Modulation signal for the topological charge. (c) Simulated displacement in the y direction retrieved at $y = 0$, $x = 2$ mm and $z = F$. (d) (color map) Dispersion relation obtained by double FFT of the temporal signals along the x direction, and (white dashed) theoretical dispersion relation of the phantom.

4 Conclusions

We have presented two biomedical applications of acoustic vortices.

On the one hand, it has been developed a proof-of-concept of a new method of elastography based on the transfer of orbital angular momentum from a vortex beam to soft tissues, either using a lens or a phased array to generate the vortex beam. With this method the tissue can be twisted, in addition to pushed as it happens with conventional systems. Then, by time modulating the ultrasound beam, shear waves can be efficiently generated. Finally, by tracking the shear waves, the elasticity of the medium can be obtained in a robust way. In addition, by the temporal modulation of the sign of the topological charge of the vortex, e.g., by using a phased array to synthesize the vortex beam, the direction of rotation of the torque can be controlled. Thus, the forced excitation can be harmonic or follow an arbitrary waveform, as a sine-sweep excitation, enabling the efficient generation of shear waves of high amplitude with controlled polarization. This technique results in a robust excitation of shear waves with quasi-omnidirectional radiation pattern and arbitrary waveform, which have a great potential to improve the imaging quality of ultrasound elastography.

On the other hand, we explored the application of acoustic holograms to physically encode time-reversed fields containing phase dislocations and, simultaneously, the phase aberrations produced by the transcranial propagation. This results in the capability of focusing acoustic vortices inside the human head for therapeutic purposes with great accuracy using very simple and compact ultrasonic systems.

This work will pave the road to design low-cost particle trapping applications, clot manipulation, torque exertion in the brain and acoustic-radiation-force based biomedical applications, opening the path to explore the biological response of the tissues to therapeutic ultrasonic vortex beams.

Acknowledgements

This research has been supported by the Spanish Ministry of Science, Innovation and Universities through grants “Juan de la Cierva – Incorporación” IJC2018-037897-I, by the Agència Valenciana de la Innovació through grants INNVA1/2020/92, INNVAL10/19/016 and INNCON/2020/009, and by Generalitat Valenciana through grant ACIF/2017/045. Action co-financed by the European Union through the Programa Operativo del Fondo Europeo de Desarrollo Regional (FEDER) of the Comunitat Valenciana IDIFEDER/2018/022.

References

[1] J. L. Thomas and R. Marchiano, "Pseudo angular momentum and topological charge conservation for nonlinear acoustical vortices," *Phys. Rev. Lett.*, vol. 91, no. 24, p. 244302, 2003, doi: 10.1103/PhysRevLett.91.244302.

[2] K. Volke-Sepúlveda, A. O. Santillán, and R. R. Boullosa, "Transfer of angular momentum to matter from acoustical vortices in free space," *Phys. Rev. Lett.*, vol. 100, no. 2, p. 24302, 2008, doi: 10.1103/PhysRevLett.100.024302.

[3] A. Riaud, M. Baudoin, J. L. Thomas, and O. Bou Matar, "Cyclones and attractive streaming generated by acoustical vortices," *Phys. Rev. E - Stat. Nonlinear, Soft Matter Phys.*, vol. 90, no. 1, p. 13008, 2014, doi: 10.1103/PhysRevE.90.013008.

[4] J. Wu, "Acoustical tweezers," *J. Acoust. Soc. Am.*, vol. 89, no. 5, pp. 2140–2143, 1991, doi: 10.1121/1.400907.

[5] D. Baresch, J.-L. Thomas, and R. Marchiano, "Observation of a Single-Beam Gradient Force Acoustical Trap for Elastic Particles: Acoustical Tweezers," *Phys. Rev. Lett.*, vol. 116, no. 024301, 2016.

[6] A. Marzo, M. Caleap, and B. W. Drinkwater, "Acoustic Virtual Vortices with Tunable Orbital Angular Momentum for Trapping of Mie Particles," *Phys. Rev. Lett.*, vol. 120, no. 4, p. 44301, 2018, doi: 10.1103/PhysRevLett.120.044301.

[7] D. G. Grier, "A revolution in optical manipulation," *Nature*, vol. 424, no. 6950, pp. 810–816, 2003, doi: 10.1038/nature01935.

[8] M. B. O. B. L. B. J.-L. T. A Riaud, "Selective manipulation of microscopic particles with precursors swirling rayleigh waves," *Phys. Rev. Appl.*, vol. 7, p. 024007, 2017.

[9] M. A. Ghanem *et al.*, "Noninvasive acoustic manipulation of objects in a living body," *Proc. Natl. Acad. Sci. U. S. A.*, 2020, doi: 10.1073/pnas.2001779117.

[10] D. Baresch and V. Garbin, "Acoustic trapping of microbubbles in complex environments and controlled payload release," *Proc. Natl. Acad. Sci. U. S. A.*, 2020, doi: 10.1073/pnas.2003569117.

[11] B. T. Hefner and P. L. Marston, "An acoustical helicoidal wave transducer with applications for the alignment of ultrasonic and underwater systems," *J. Acoust. Soc. Am.*, vol. 106, no. 6, pp. 3313–3316, 1999, doi: 10.1121/1.428184.

[12] N. Jiménez, R. Picó, V. Sánchez-Morcillo, V. Romero-García, L. M. García-Raffi, and K. Staliunas, "Formation of high-order acoustic Bessel beams by spiral diffraction gratings," *Phys. Rev. E*, vol. 94, no. 5, p. 053004, Nov. 2016, doi: 10.1103/PhysRevE.94.053004.

[13] N. Jiménez, V. Romero-García, L. M. García-Raffi, F. Camarena, and K. Staliunas, "Sharp acoustic vortex focusing by Fresnel-spiral zone plates," *Appl. Phys. Lett.*, vol. 112, no. 20, p. 204101, May 2018, doi: 10.1063/1.5029424.

[14] S. Gspan, A. Meyer, S. Bernet, and M. Ritsch-Marte, "Optoacoustic generation of a helicoidal ultrasonic beam," *J. Acoust. Soc. Am.*, vol. 115, no. 3, pp. 1142–1146, 2004, doi: 10.1121/1.1643367.

[15] R. D. Muelas-Hurtado, J. L. Ealo, J. F. Pazos-Ospina, and K. Volke-Sepúlveda, "Generation of multiple vortex beam by means of active diffraction gratings," *Appl. Phys. Lett.*, vol. 112, no. 8, p. 84101, 2018, doi: 10.1063/1.5016864.

[16] X. Jiang, Y. Li, B. Liang, J. C. Cheng, and L. Zhang, "Convert Acoustic Resonances to Orbital Angular Momentum," *Phys. Rev. Lett.*, vol. 117, no. 3, p. 34301, 2016, doi: 10.1103/PhysRevLett.117.034301.

[17] K. Melde, A. G. Mark, T. Qiu, and P. Fischer, "Holograms for acoustics," *Nature*, vol. 537, no. 7621, p. 518, 2016.

[18] S. Jiménez-Gambín, N. Jiménez, J. M. Benlloch, and F. Camarena, "Holograms to Focus Arbitrary Ultrasonic Fields through the Skull," *Phys. Rev. Appl.*, vol. 12, no. 1, p. 014016, Jul. 2019, doi: 10.1103/PhysRevApplied.12.014016.

[19] M. Ferri *et al.*, "On the Evaluation of the Suitability of the Materials Used to 3D Print Holographic Acoustic Lenses to Correct Transcranial Focused Ultrasound Aberrations," *Polymers (Basel).*, vol. 11, no. 9, p. 1521, Sep. 2019, doi: 10.3390/polym11091521.

[20] S. Jiménez-Gambín, N. Jiménez, J. M. Benlloch, and F. Camarena, "Generating Bessel beams with broad depth-of-field by using phase-only acoustic holograms," *Sci. Rep.*, vol. 9, no. 1, p. 20104, Dec. 2019, doi: 10.1038/s41598-019-56369-z.

[21] B. E. Treeby and B. T. Cox, "Modeling power law absorption and dispersion for acoustic propagation using the fractional Laplacian," *J. Acoust. Soc. Am.*, vol. 127, no. 5, pp. 2741–2748, 2010.